Australian Journal of Earth Sciences: An International Geoscience Journal of the Geological Society of Australia
Publication details, including instructions for authors and subscription information:
http://www.tandfonline.com/loi/taje20

Triassic asymmetric subduction rollback in the southern New England Orogen (eastern Australia): the end of the Hunter-Bowen Orogeny

P-F. Li [a], G. Rosenbaum [a] & D. Rubatto [b]

[a] School of Earth Sciences, University of Queensland, Brisbane 4072, Queensland, Australia

[b] Research School of Earth Sciences, Australian National University, Canberra, 0200 ACT, Australia

Version of record first published: 30 Jul 2012.

To cite this article: P-F. Li, G. Rosenbaum & D. Rubatto (2012): Triassic asymmetric subduction rollback in the southern New England Orogen (eastern Australia): the end of the Hunter-Bowen Orogeny, Australian Journal of Earth Sciences: An International Geoscience Journal of the Geological Society of Australia, 59:6, 965-981

To link to this article: http://dx.doi.org/10.1080/08120099.2012.696556

Australian Journal of Earth Sciences (2012) **59**, (965–981)

Triassic asymmetric subduction rollback in the southern New England Orogen (eastern Australia): the end of the Hunter-Bowen Orogeny

P-F. LI[1], G. ROSENBAUM[1] AND D. RUBATTO[2]

[1]*School of Earth Sciences, University of Queensland, Brisbane 4072, Queensland, Australia.*
[2]*Research School of Earth Sciences, Australian National University, Canberra, 0200 ACT, Australia.*

The New England Orogen, the youngest subduction-related component in the Australian continent, records a prolonged history of west-dipping subduction from the Devonian to the Triassic. From mid–late Permian (*ca* 265 Ma) to Upper Triassic (*ca* 235 Ma), the New England Orogen was subjected to pronounced contractional deformation (Hunter-Bowen Orogeny) and widespread I-type calc-alkaline magmatism. We obtained zircon U–Pb ages from seven granitic samples within the I-type magmatic system. The new SHRIMP U–Pb data ranging from 255 to 215 Ma, combined with previous geochronological data from the southern New England Orogen, suggest that magmatism during the Hunter-Bowen Orogeny was spatially distributed along a NNE–SSW belt that was likely associated with a west-dipping Andean-type subduction zone. In contrast, younger magmatism (235–215 Ma) is aligned along a N–S belt farther east. Assuming that magmatism was subduction-related and was spatially distributed parallel to the subduction zone, we interpret the spatio-temporal change in magmatism as an indicator for eastward arc migration, possibly in response to slab rollback. The trench position is not well constrained but was possibly located between the Australian continent and the Lord Howe Rise. We propose a model involving asymmetric slab rollback, possibly in response to pinning of the northern part of subduction zone by the Gympie Terrane accretion. Our model invokes that this phase of tectonic activity marked the transition from contractional deformation in the continental margin to extensional tectonics that represents the earliest phase of the Mesozoic rifting of eastern Australia.

KEY WORDS: New England Orogen, New England Batholith, Hunter-Bowen Orogeny, Subduction rollback, Eastern Australia.

INTRODUCTION

Subduction zones are commonly associated with episodic transitions from arc-perpendicular contraction (trench advance) to extension (trench rollback) (Royden 1993). This behaviour has likely played a role in the tectonic evolution of eastern Australia (Collins 2002; Jenkins *et al.* 2002), but the exact timing of such transitions and their geodynamic driving mechanisms are still not fully understood.

The New England Orogen (NEO), the easternmost and youngest orogenic component in Australia (Figure 1), is one place where this episodic behaviour can be investigated. Jenkins *et al.* (2002) suggested that the NEO was subjected to episodes of contraction and extension related to alternating periods of trench advance and trench rollback. One of the most pronounced contractional events, commonly referred as the Hunter-Bowen Orogeny (Carey & Browne 1938; Korsch *et al.* 2009c), was accompanied by widespread I-type calc-alkaline magmatism (Shaw & Flood 1981, 2009; Bryant *et al.* 1997; Shaw *et al.* 2011). However, the fundamental geodynamics associated with the Hunter-Bowen Orogeny, and its relationship with the temporal and spatial distribution of the Permian–Triassic magmatism, are still unclear. This event was followed by the development of a series of basins (e.g. Ipswich Basin), possibly in response to subduction rollback (Jenkins *et al.* 2002). However, the exact timing and nature of the transition from contraction to extension are not well constrained.

In this paper, we provide new SHRIMP U–Pb data on a number of late Permian and Triassic granitoids from the southern NEO. We discuss these results in the context of the spatio-temporal distribution of late Permian to Triassic magmatic rocks in the southern NEO, and we propose that the end of the Hunter-Bowen Orogeny, at *ca* 235 Ma, marked a major tectonic transition from contraction to extension.

GEOLOGICAL SETTING

The NEO evolved in the Paleozoic convergent margin of eastern Gondwana (Cawood 2005; Glen 2005) and extends over ~1500 km along the coast of eastern Australia. It is normally subdivided into a northern segment (in Queensland) and a southern segment (in southern Queensland and northern New South Wales), which

*Corresponding author: pengfei.li@uqconnect.edu.au

ISSN 0812-0099 print/ISSN 1440-0952 online
http://dx.doi.org/10.1080/08120099.2012.696556

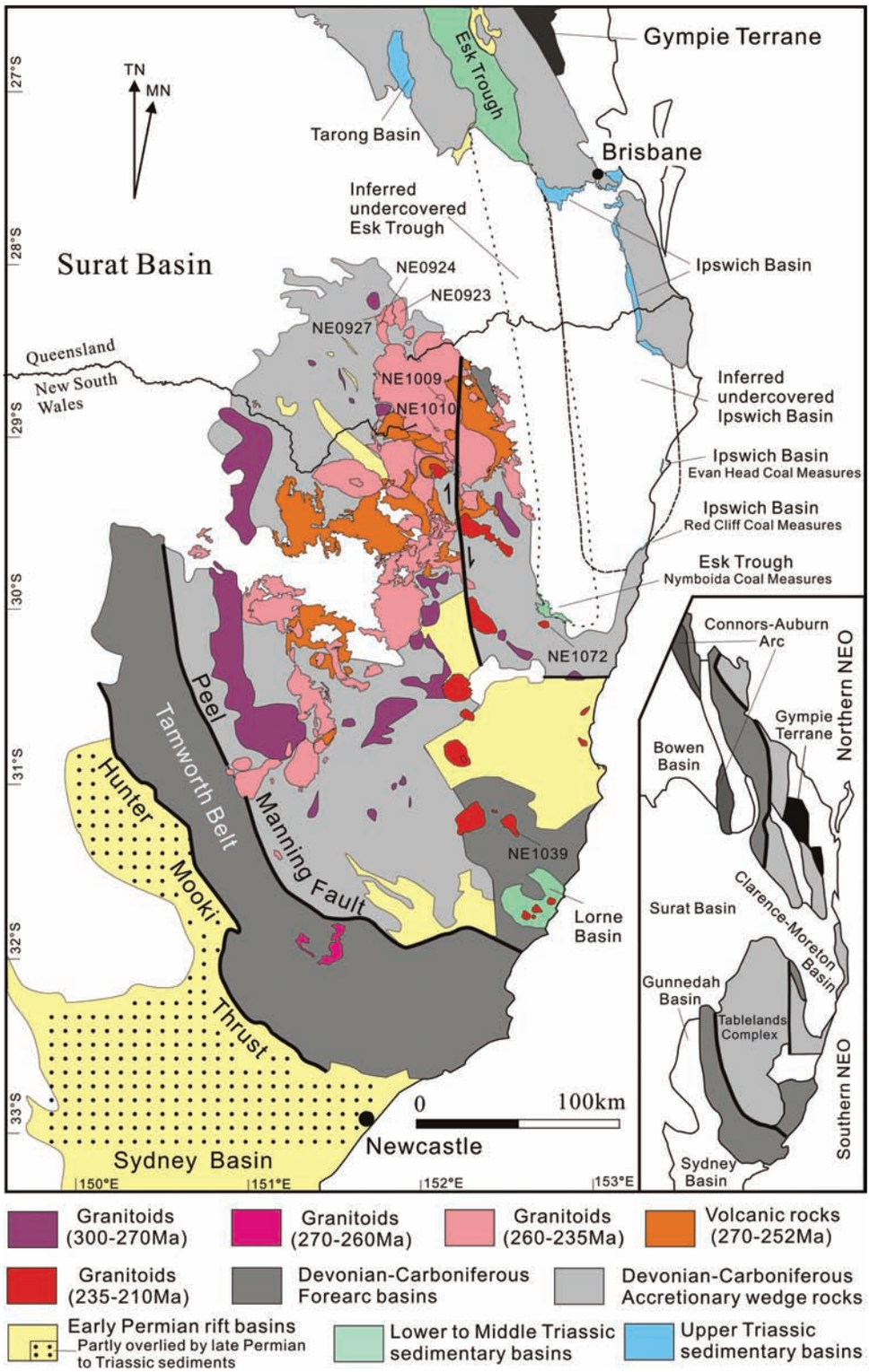

Figure 1 Regional geological map of the southern NEO based on the 1:500,000 map sheet (Moreton), 1:250,000 map sheets (Singleton, Newcastle, Tamworth, Hastings, Manilla, Dorrigo–Coffs Harbour, Inverell and Grafton), and 1:100,000 map sheets (Stanthorpe and Allora). Inset map shows the main tectonic elements in the NEO. The outcrop locations of the Esk Trough and Ipswich Basin are based on Scheibner (1998), and the locations of these basins under the Clarence-Moreton Basin are after Harrington & Korsch (1985), Roach (1997) and Phillips *et al.* (2011).

are separated by the Mesozoic Clarence-Moreton Basin (Figure 1). The majority of the rocks in the orogen are Devonian to Carboniferous successions attributed to three components of a subduction zone. These are, from west to east, a Devonian–Carboniferous volcanic arc, a forearc basin and an accretionary wedge (Figure 1). The

volcanic arc is exposed in the northern NEO (Connors–Auburn Arc), but is mostly lacking in the southern NEO, where it is inferred to be concealed under younger sedimentary rocks. To the east of the arc, forearc basin and accretionary wedge rocks are exposed in both the northern and southern NEO (Figure 1). In the southern NEO, the forearc basin (Tamworth Belt) is separated from the accretionary wedge (Tablelands Complex) by the Peel–Manning Fault System (Leitch 1974; Korsch 1977). In a map view, both the Tamworth Belt and Tablelands Complex are strongly curved, and define a series of oroclines (Korsch & Harrington 1987; Cawood *et al.* 2011b; Li *et al.* 2012; Rosenbaum 2012; Rosenbaum *et al.* 2012).

The Devonian to Carboniferous elements of the orogenic belt are partially overlain by early Permian clastic sedimentary and volcanic rocks (Roberts *et al.* 1996). These strata have supposedly been deposited in rift basins that formed during a period of widespread extension (Leitch 1988; Korsch *et al.* 2009b), possibly in response to subduction rollback (Jenkins *et al.* 2002; Rosenbaum *et al.* 2012). Leitch (1988) suggested that in the southern NEO, the early Permian basins east of the Peel-Manning Fault System (Figure 1) have originally developed in a single basin, termed the Barnard Basin. Volcanic material at the bottom of these basins has been dated at 293–291 Ma (Roberts *et al.* 1996; Cawood *et al.* 2011a). Basin formation was coeval with the emplacement of a large volume of S-type granitoids (the Bundarra and Hillgrove suites; Figure 2), which have recently been dated as 296–288 Ma by U–Pb SHRIMP geochronology (Cawood *et al.* 2011a; Rosenbaum *et al.* 2012). This period also overlapped with oroclinal bending, which may have resulted from along-strike variations in subduction rollback (Li *et al.* 2012; Rosenbaum *et al.* 2012). The Sydney, Gunnedah and Bowen basins (Figure 1) possibly represent back arc extensional basins that developed at the overriding plate in response to this phase of subduction rollback (Rosenbaum *et al.* 2012). These basins developed along a N–S rift system during the early Permian (Danis *et al.* 2010, 2011), and evolved into a subsidence phase of sedimentation driven by thermal relaxation at *ca* 280 Ma (Korsch *et al.* 2009b). To the east of the NEO, the allochthonous Gympie Terrane (Figure 1), interpreted as an exotic early Permian offshore arc, was accreted to the Australian continent in the Triassic (Harrington & Korsch 1985; Harrington 2008).

Contractional deformation associated with the Hunter-Bowen Orogeny commenced at *ca* 265 Ma (Carey & Browne 1938; Collins 1991; Holcombe *et al.* 1997; Korsch *et al.* 2009c). This phase of deformation was at least partly accompanied by the emplacement of I-type calc-alkaline granitoids and volcanic rocks in the southern NEO (Table 1). The spatial distribution of this magmatic belt follows broadly a NNE–SSW trend (Figure 1).

The Hunter-Bowen phase of deformation in the northern NEO began at *ca* 265 Ma and ceased prior to *ca* 228 Ma, as constrained by the age of flat lying volcanic rocks above folded sedimentary strata in the Esk Trough (Holcombe *et al.* 1997). In the southern NEO, the timing of deformation is relatively poorly constrained. Contractional deformation related to the Hunter-Bowen Orogeny mainly involved: (1) westward propagation of foreland thrust deformation into the Sydney–Gunnedah Basins (Korsch *et al.* 2009c), with the eastern margin of the basins delineated by the dominantly east-dipping Hunter-Mooki Thrust (Figure 1). The exact timing of activity along the Hunter-Mooki Thrust is not well constrained. A horizontal tuff layer, overlying the Lochinvar anticline in the Sydney Basin, yielded a U–Pb age of 256 ± 4 Ma (Gulson *et al.* 1990; Glen & Beckett 1997), providing a minimum age constraint for the end of the Permian Hunter-Mooki Thrust in this region; (2) west-directed thrusting in the Devonian to Carboniferous forearc rocks of the Tamworth Belt (Woodward 1995); (3) west-dipping, high-angle reverse faulting in the southern NEO, which exhumed lower amphibolite facies mylonites that yielded a Rb–Sr age of 266–258Ma (Landenberger *et al.* 1995); and (4) folding and low-grade metamorphism in the early Permian Nambucca Block at 264–260 Ma, as constrained by whole-rock $^{40}Ar/^{39}Ar$ analysis (Offler & Foster 2008).

During the Lower to Middle Triassic, sedimentary basins were developed in eastern Australia, including the Lorne Basin and Esk Trough (Figures 1, 2). The Lorne Basin is a relatively small circular-shaped basin ($\sim$ 35 km in diameter) that is filled predominantly with Lower Triassic clastic sedimentary rocks with indicative plant fossils (Pratt 2010). The Esk Trough is filled with a terrestrial sequence of volcaniclastic rocks and interbedded clastic sedimentary rocks, including an alluvial and lacustrine sequence (Cranfield *et al.* 1976; Holcombe *et al.* 1997). The Middle Triassic (Anisian to Ladinian) age of the Esk Trough sedimentary rocks was determined on the basis of plants fossils (De Jersey 1972; Helby *et al.* 1987). A coeval stratigraphic succession with correlative macrofloras was found in the Nymboida Coal Measures farther south (Figure 1; Flint & Gould 1975; Webb 2001), and it is therefore possible that the Esk Trough extended southward into the area that is currently covered by the Clarence-Moreton Basin (Figure 1). Structurally, the Esk Trough is characterised by asymmetric half-grabens that could have formed by oblique rifting in response to dextral transtension (Korsch *et al.* 1989). The Esk Trough also records a phase of NW–SE trending folding, which is possibly associated with a late stage of the Hunter-Bowen Orogeny (Holcombe *et al.* 1997).

A series of Upper Triassic basins (e.g. the Ipswich and Tarong basins) were developed in areas adjacent to the southern NEO (Figure 1), and were accompanied by dextral strike-slip faulting (e.g. the Demon Fault; Korsch *et al.* 1978; McPhie & Fergusson 1983). Half-graben fault geometries and bimodal volcanism in these basins are indicative of an extensional environment (Holcombe *et al.* 1997). The Ipswich Basin is overlain by the Clarence-Moreton Basin, but crops out along the edge of the latter (Figure 1). In the southern margin of the NEO, the Lorne Basin continued to develop during the Upper Triassic, with basin fill including rhyolites and airfall tuff (Graham *et al.* 2006; Pratt 2010). Coeval with the development of these Upper Triassic basins, granitoids were emplaced along a discontinuous belt with the map-view N–S orientation (Figures 1, 2; Table 1).

The youngest sedimentary basins in the area of the southern NEO are the Clarence-Moreton and Surat Basins. The former started to develop in the latest Upper

Table 1 Timing of Permian–Triassic magmatic rocks in the southern New England Orogen.

	Supersuite	Name	Age (Ma)	Method	Reference
1	Clarence River	Barrington Tops Granodiorite	267.2 ± 1.4	U–Pb SHRIMP	Cawood *et al.* (2011a)
2	Wandsworth Volcanic Group	Drake Volcanics	264.4 ± 2.5	U–Pb SHRIMP	Cross *et al.* (2010)
3	———————	Mingimarny Granite	260.1 ± 2.4	U–Pb SHRIMP	Cross *et al.* (2009)
4	———————	Boxwell Granite	256.6 ± 1.7	U–Pb SHRIMP	Cross *et al.* (2010)
5	Herries	Palgrave Granite	256 ± 1.8	U–Pb SHRIMP	Donchak *et al.* (2007)
6	Clarence River	Dumbudgery Creek Granodiorite	259–252	Ar–Ar (hornblende)	Bryant *et al.* (1997b)
7	Clarence River	Towgon Grange Granodiorite	*ca* 257.5	Ar–Ar (hornblende)	Bryant *et al.* (1997b)
8	Wandsworth Volcanic Group	Dundee Rhyodacite	257.6 ± 2.5	La-ICP-MS U–Pb	Belousova *et al.* (2006)
			254.34 ± 0.34	TIMS U–Pb	Brownlow & Cross (2010)
9	Uralla	Parlour Mountain Granite	254.7 ± 1.6	U–Pb SHRIMP	Cross *et al.* (2010)
			ca 251	Rb–Sr (biotite)	Shaw (1994)
10	Wandsworth Volcanic Group	Wallangarra Volcanics	253 ± 2.4	U–Pb SHRIMP	Cross *et al.* (2009)
11	Moonbi	Walcha Road Monzogranite	253.8 ± 1.8	U–Pb SHRIMP	Geoscience Australia dataset*
			249 ± 3	La-ICP-MS U–Pb	Jackson *et al.* (2004)
12	**Herries**	**Fairleigh Granite**	**253.3 ± 2.5**	**U–Pb SHRIMP**	**This study**
13	**Herries**	**Clare Hills Granite**	**252.0 ± 2.5**	**U–Pb SHRIMP**	**This study**
14	Clarence River	Duncans Creek Trondhjemite	252–249	U–Pb SHRIMP	Cawood *et al.* (2011)
15	**Herries**	**Herries Granite**	**251.8 ± 2.5**	**U–Pb SHRIMP**	**This study**
16	Stanthrope	Mackenzie Monzogranite	251.7 ± 2.1	U–Pb SHRIMP	Geoscience Australia dataset*
17	Uralla	Tingha Monzogranite	251.3 ± 1.7	U–Pb SHRIMP	Cross *et al.* (2010)
			ca 249	Rb–Sr (biotite)	Shaw (1994)
18	Mole	Gilgai Granite	254–250	U–Pb SHRIMP	Cross *et. al* (2010)
			247–243	Rb–Sr (biotite)	Shaw (1994)
19	Moonbi	Inlet Monzonite	255–249	U–Pb SHRIMP	Geoscience Australia dataset*
20	———————	Koreelan Creek Granodiorite	250.5 ± 1.4	Ar–Ar (hornblende)	Bryant *et al.* (1997b)
21	Clarence River	Jenny Lind Granite	249.7	Ar–Ar (hornblende)	Bryant *et al.* (1997b)
22	Mole	Mole Granite	246 ± 2		Kleeman *et al.* (1997)
23	Stanthrope	Mount Mitchell Monzogranite	249–243	Rb–Sr (biotite)	Shaw (1994)
24	Moonbi	Oban River Leucomonzogranite	*ca* 248	Rb–Sr (biotite)	Shaw (1994)
25	Uralla	Wards Mistake Monzogranite	248–244	Rb–Sr (biotite)	Shaw (1994)
26	———————	Highlands Monzonite	247–245	Rb–Sr (biotite)	Shaw (1994)
27	———————	Pine Tree Adamellite	*ca* 248	Rb–Sr (biotite)	Shaw (1994)
28	Uralla	Booralong Adamellite	*ca* 250	Rb–Sr (biotite)	Shaw (1994)
29	Uralla	Mount Duval Monzogranite	252–245	Rb–Sr (biotite)	Shaw (1994)
30	Uralla	Glenore Monzogranite	250–247	Rb–Sr (biotite)	Shaw (1994)
31	Uralla	Gwydir River Monzogranite	249–244	Rb–Sr (biotite)	Shaw (1994)
			252.3 ± 1.5	U–Pb SHRIMP	Cross *et al.* (2010)
32	Uralla	Yarrowyck Granodiorite	250–246	Rb–Sr (biotite)	Shaw (1994)
33	Uralla	Uralla Granodiorite	251–246	Rb–Sr (biotite)	Shaw (1994)
34	Moonbi	Looanga Monzogranite	*ca* 247	Rb–Sr (biotite)	Shaw (1994)
35	Moonbi	Attunga Creek Monzogranite	*ca* 249	Rb–Sr (biotite)	Shaw (1994)
36	Moonbi	Moonbi Monzogranite	250–247	Rb–Sr (biotite)	Shaw (1994)
37	Uralla	Kentucky Diorite	252–245	Rb–Sr (biotite)	Shaw (1994)
38	Uralla	Terrible Vale Porphyritic Microtonalite	251–247	Rb–Sr (biotite)	Shaw (1994)

(*continued*)

Table 1 (*Continued*).

	Supersuite	Name	Age (Ma)	Method	Reference
39	Uralla	Shalimar Tonalite	247–246	Rb–Sr (biotite)	Shaw (1994)
40	Moonbi	Bendemeer Monzogranite	*ca* 247	Rb–Sr (biotite)	Shaw (1994)
41	**Herries**	**Boonoo Granite**	**245.6±2.5**	**U–Pb SHRIMP**	**This study**
42	Stanthrope	Sandy Flat Monzogranite	247–244	Rb–Sr (biotite)	Shaw (1994)
43	Moonbi	Red Range Microleucogranite	*ca* 245	Rb–Sr (biotite)	Shaw (1994)
44	Uralla	The Basin Monzogranite	*ca* 245	Rb–Sr (biotite)	Shaw (1994)
45	Moonbi	Limbri Leucomonzogranite	*ca* 245	Rb–Sr (biotite)	Shaw (1994)
46	Uralla	Back Creek Tonalite	*ca* 245	Rb–Sr (biotite)	Shaw (1994)
47	Stanthrope	Stanthrope Granite	243–238	Rb–Sr (biotite)	Shaw (1994)
			246.9±2.0	U–Pb SHRIMP	Donchak *et al.* (2007)
48	Herries	Maryland granite	243–241	Rb–Sr (biotite)	Shaw (1994)
49	Stanthrope	Undercliffe Falls Monzogranite	*ca* 245	Rb–Sr (biotite)	Shaw (1994)
50	Stanthrope	Bungulla Monzogranite	248–243	Rb–Sr (biotite)	Shaw (1994)
51	Stanthrope	Nonnington Leucomonzogranite	*ca* 240	Rb–Sr (biotite)	Shaw (1994)
52	———	Petries Sugarloaf Leucoadamellite	*ca* 242	Rb–Sr (biotite)	Shaw (1994)
53	Stanthrope	Mount Jonblee Leucomonzogranite	*ca* 243	Rb–Sr (biotite)	Shaw (1994)
54	Stanthrope	Bolivia Range Leucomonzogranite	*ca* 241	Rb–Sr (biotite)	Shaw (1994)
55	Moonbi	Kingsgate Leucogranite	246–243	Rb–Sr (biotite)	Shaw (1994)
56	Mole	Dumboy-Gragin Granite	243±3.7	U–Pb SHRIMP	Vickery *et al.* (1997)
57	———	**Bookookoorara Monzogranite**	**240.1±2.4**	**U–Pb SHRIMP**	**This study**
58	Stanthrope	Billyrimba Leucomonzogranite	235–233	Rb–Sr (biotite)	Shaw (1994)
59	Stanthrope	Dandahra Creek Leucogranite	235–233	Rb–Sr (biotite)	Shaw (1994)
60	———	Chaelundi Leucomonnzogranite	233±3	U–Pb (zircon)	Phillips *et al.* (2011)
			235–232	Rb–Sr (biotite)	Shaw (1994)
61	Round Mountain	Round Mountain Leucoadamellite	*ca* 227	Rb–Sr (biotite)	Shaw (1994)
62	———	Valla Adamellite	225–222	Rb–Sr (biotite)	Shaw (1994)
63	Round Mountain	Yarrahapinni Adamellite	225–222	Rb–Sr (biotite)	Shaw (1994)
64	Round Mountain	Carrai Granodiorite	227–224	Rb–Sr (biotite)	Shaw (1994)
65	Uralla	Botumburra Range Adamellite	228–226	Rb–Sr (biotite)	Shaw (1994)
66	———	**Nymboi Granite (new name)**	**221.3±2.2**	**U–Pb SHRIMP**	**This study**
67	———	**Gundle Granite**	**217.1±2.2**	**U–Pb SHRIMP**	**This study**

*Geoscience Australia SHRIMP U–Pb Geochronology Interim Data Release July 2007.

Triassic and continued to develop until the Lower and Middle Jurassic in response to regional subsidence (Day *et al.* 1983; O'Brien *et al.* 1994). Sedimentation in the Surat Basin farther west initiated in the Lower Jurassic and continued until the Lower Cretaceous (Totterdell *et al.* 2009; Waschbusch *et al.* 2009). This was followed by the opening of the Tasman Sea in the late Mesozoic to early Cenozoic (Hayes & Ringis 1973), which separated the Lord Howe Rise (including parts of the NEO and the Lachlan Orogen) from the Australian continent (Harrington 2008).

U–PB GEOCHRONOLOGY

Sample description

Samples were selected from granitic rocks with the aim of better constraining the spatio-temporal relationships between the NNE–SSW and N–S magmatic belts (Figure 1). We collected samples from seven different plutons located along the N–S belt and at the intersection of the two belts (Figure 1). The samples are mostly granites and monzogranites. The Herries Granite (NE0923), Fairleigh Granite (NE0924), Clare Hills Granite (NE0927), Boonoo Granite (NE1010), Gundle Granite (NE1039) and Nymboi Granite (new name, NE1072) predominantly consist of biotite, quartz, feldspar and minor hornblende. Sample NE1009, from the large pluton of Bookookoorara Monzogranite, contains biotite, quartz, K-feldspar and plagioclase.

Analytical techniques

Zircon grains were separated using conventional crushing, heavy liquid and magnetic techniques. The grains were mounted in epoxy resin and polished to expose a near equatorial section. Cathodoluminescence (CL) investigation was carried out on two different scanning electron microscopes equipped with ellipsoidal mirrors: a HITACHI S2250N and a JEOLJSM-6610A operating at similar conditions of 15 kV and 20 mm working distance.

Zircons were analysed for U, Th and Pb using the sensitive high-resolution ion microprobes (SHRIMP II and SHRIMP RG) at the Australian National University in Canberra. Instrumental conditions and data acquisition are described by Williams (1998). Data were collected in sets of six scans throughout the masses, and a reference zircon was measured every fourth analysis. U–Pb data were collected over several analy-

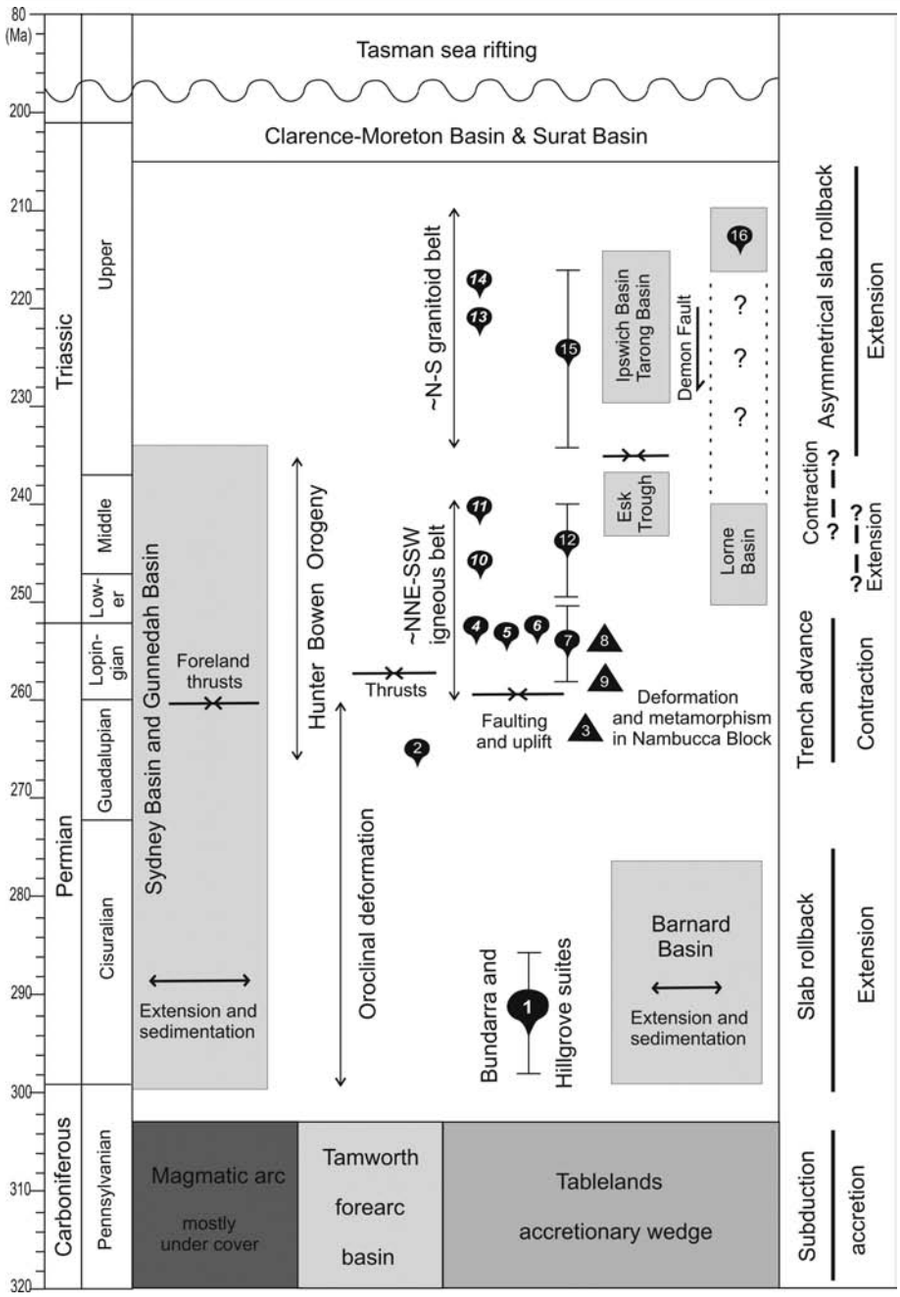

Figure 2 Schematic time–space diagram for the southern NEO and adjacent regions (partly modified after Cawood *et al.* 2011a). Data sources: 1– Bundarra and Hillgrove suites (Cawood *et al.* 2011a; Rosenbaum *et al.* 2012); 2 – Barrington Top Granodiorite (267.2±1.4) (Cawood *et al.* 2011a); 3 – Drake Volcanics (264.4±2.5 Ma) (Cross & Blevin 2010) ; 4 – Clare Hills Granite (this study); 5 – Fairleigh Granite (this study); 6 – Herries Granite (this study); 7 – Other plutons at 260–251 Ma based on published age data (see Table 1); 8 – Dundee Rhyodacite (254.34±0.34 Ma) (Brownlow & Cross 2010); 9 – Emmaville Volcanics, overlain by late Permian Dundee Rhyodacite (Stewart 2001); 10 – Boonoo Granite (this study); 11 – Bookookoorara Monzogranite (this study); 12 – Other plutons at 251–240 Ma based on published age data (see Table 1); 13 – Nymboi Granite (this study); 14 – Gundle Granit (this study); 15 – Other plutons at 235–215 Ma based on published age data (see Table 1); 16 – Middle Brother Diorite. Triangle represents volcanic rocks.

tical sessions using the same standard. Analytical sessions had a calibration error between 1.4 and 2.1% (2 sigma), which was propagated to single analyses. The measured $^{206}Pb/^{238}U$ ratio was corrected using reference zircon from the Temora granodiorite (TEM, Black *et al.* 2003). The analyses were corrected for common Pb using three different methods based on ^{204}Pb, ^{207}Pb and ^{208}Pb (Williams 1998). All three corrections returned results that are identical within error. The common Pb composition was assumed to be that predicted by the model of Stacey & Kramers (1975). We present data on concordia diagrams based on the ^{204}Pb common Pb correction and report weighted mean $^{206}Pb/^{238}U$ ages at 95% confidence level (c.l.) and relative MSWD, after exclusion of outliers. In most samples, the average $^{206}Pb/^{238}U$ ages, which typically have a 0.5–0.7% error (95% c.l.), are forced to 1% to account for external errors. Data evaluation and age calculations were done with Squid 1 and Isoplot/Excel software (Ludwig 2003).

RESULTS

Zircons from all samples are euhedral and generally elongated. Their internal structure is characterised by oscillatory zoning (Figure 3). Geochronological analyses (Table 2) were concentrated on the zircon rims. In all samples, a main data cluster is identified and the average of this cluster is interpreted as the age of granitoid crystallisation (Figure 4). In several samples, a few analyses yield apparently younger or older ages than the main cluster. These extraneous ages were excluded from the main age calculations on statistical grounds (scatter above analytical uncertainty).

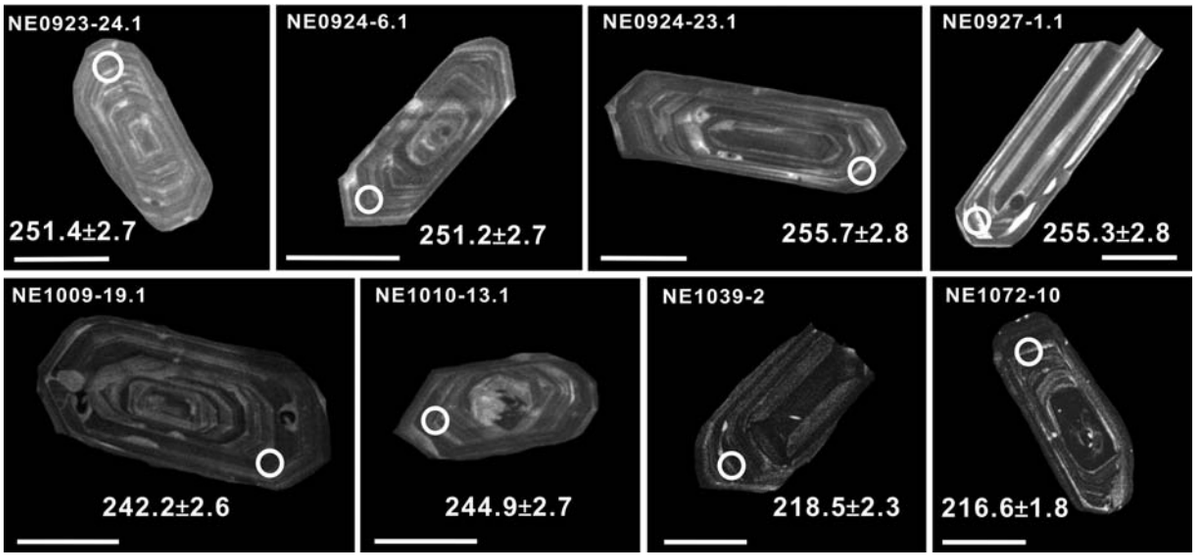

Figure 3 Cathodoluminescence images (CL) of selected zircon crystals. White scale bars are 100 mm and circles indicate the location of SHRIMP U–Pb analyses. Ages are in Ma with one sigma error.

Several of the scattering analyses are discordant or rich in common Pb; in some cases no apparent reason for exclusion could be found other than analytical scatter.

Zircon from the Farleigh Granite (NE0924) yielded ages that scatter above analytical uncertainty. The probability diagram shows some clear younger outliers and a tail to older ages. After excluding the youngest outliers and the two oldest ages, which may have sampled some inherited component, the population passes the F-test and defines an average $^{206}Pb/^{238}U$ age of 253.3±2.5 Ma with MSWD of 1.3.

Zircon analyses for the Herries Granite (NE0923) mostly cluster at *ca* 250 Ma. Four analyses that contain a high amount of common Pb returned clearly younger ages. The main data cluster (26 analyses) still scatters above analytical uncertainty, probably due to inheritance or late magmatic modification that is not detectable by textural features within the analysed zircon. After exclusion of five outliers, the main cluster of analyses passes the F-test and yields an age of 252.1±2.5 Ma (MSWD=1.6, N=21), which is interpreted as a statistically significant crystallisation age. The exclusion of outliers has no effect on the final error calculation as the internal error remains below the imposed 1% external error (see analytical techniques above).

For the Clare Hills Granite (NE0927), zircon analyses yielded ages ranging from 258 to 230 Ma. With the exclusion of a clear outlier, the remaining analyses still scatter well above analytical uncertainty (average age 249.2±2.4 Ma, MSWD=3.7). The probability diagram shows a distribution of ages skewed towards younger values, suggesting a slight disturbance of the U–Pb system. This justifies elimination of the younger analyses to satisfy the F-test, and results in an average $^{206}Pb/^{238}U$ age of 252.0±2.5 Ma (MSWD=1.5, N =17).

In the Boonoo Granite (sample NE1010), most zircon analyses (20/26) yielded a consistent average $^{206}Pb/^{238}U$ age of 245.6±2.5 Ma (MSWD=2.2). The remaining six analyses were excluded either because of high common Pb (3.5–9 wt%), and/or because their scatter was well above analytical uncertainty.

In sample NE1009 from the Bookookoorara Monzogranite, 21 zircon analyses define the main age cluster (average $^{206}Pb/^{238}U$ age of 240.1±2.4 Ma, MSWD=2.4). Five additional analyses yielded slightly older ages (average $^{206}Pb/^{238}U$ age of 253.2±2.5 Ma, MSWD=0.46) despite being on similar oscillatory-zoned zircon domains. We suggest that these zircons represent an early magmatic pulse in the same granitic body.

Zircon analyses for the Nymboi Granite (NE1072) define a main cluster with an average $^{206}Pb/^{238}U$ age of 221.3±2.2 Ma (MSWD=2.4). Five analyses, some of which have high common Pb, scatter to younger ages and are excluded from the average age calculation.

In the Gundle Granite (NE1039), oscillatory zoned zircons yielded Upper Triassic ages with an average at 217.1±2.2 Ma (MSWD=1.6, N=16). Two distinctly younger analyses were excluded.

Geochronological results of all seven samples indicate that the granitoids belong to the late Permian to Upper Triassic phase of magmatism. The samples from Clare Hills Granite, Fairleigh Granite and Herries Granite yielded late Permian/Lower Triassic ages of 252.0±2.5, 253.3±2.5 and 252.1±2.5 Ma, respectively. The ages of Bookookoorara Monzogranite and Boonoo Granite are only slightly younger (240.1±2.4 and 245.6±2.5 Ma, respectively). The Gundle Granite and Nymboi Granite yielded younger Upper Triassic ages of 217.1±2.2 and 221.3±2.2 Ma, respectively.

DISCUSSION

Late Permian shallow-dipping subduction

The ages of five granitoids dated by us are close to the Permo–Triassic boundary (Clare Hills Granite, Fairleigh Granite, Herries Granite, Bookookoorara Monzogranite and Boonoo Granite). All these granitoids are

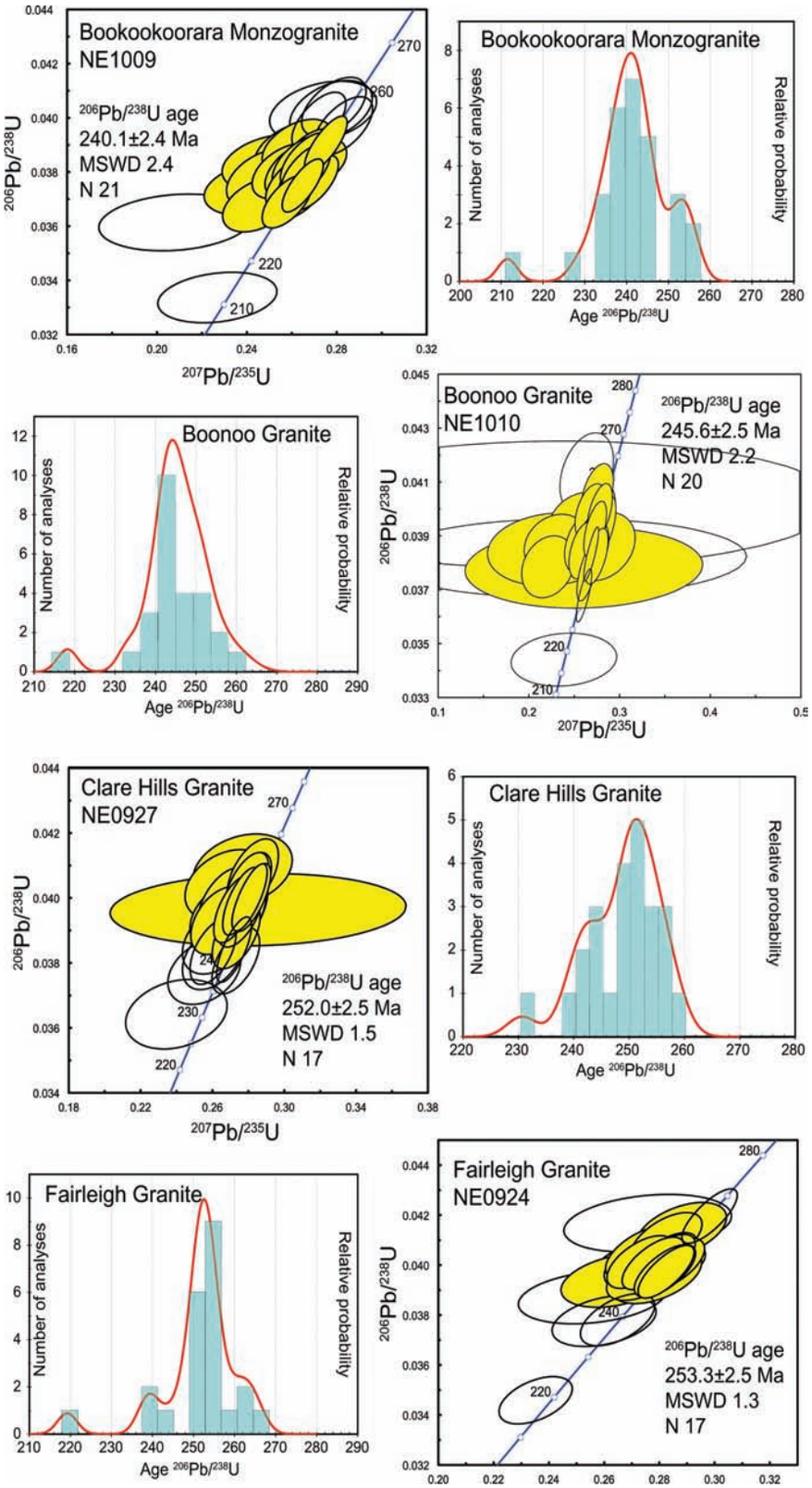

Figure 4 Concordia diagrams for zircon U–Pb analyses. Ellipses represent two sigma errors. Data plotted as unfilled ellipses were excluded from the average age calculation. The reported $^{206}Pb/^{238}U$ ages are weighted average with relative MSWD and number of analyses averaged.

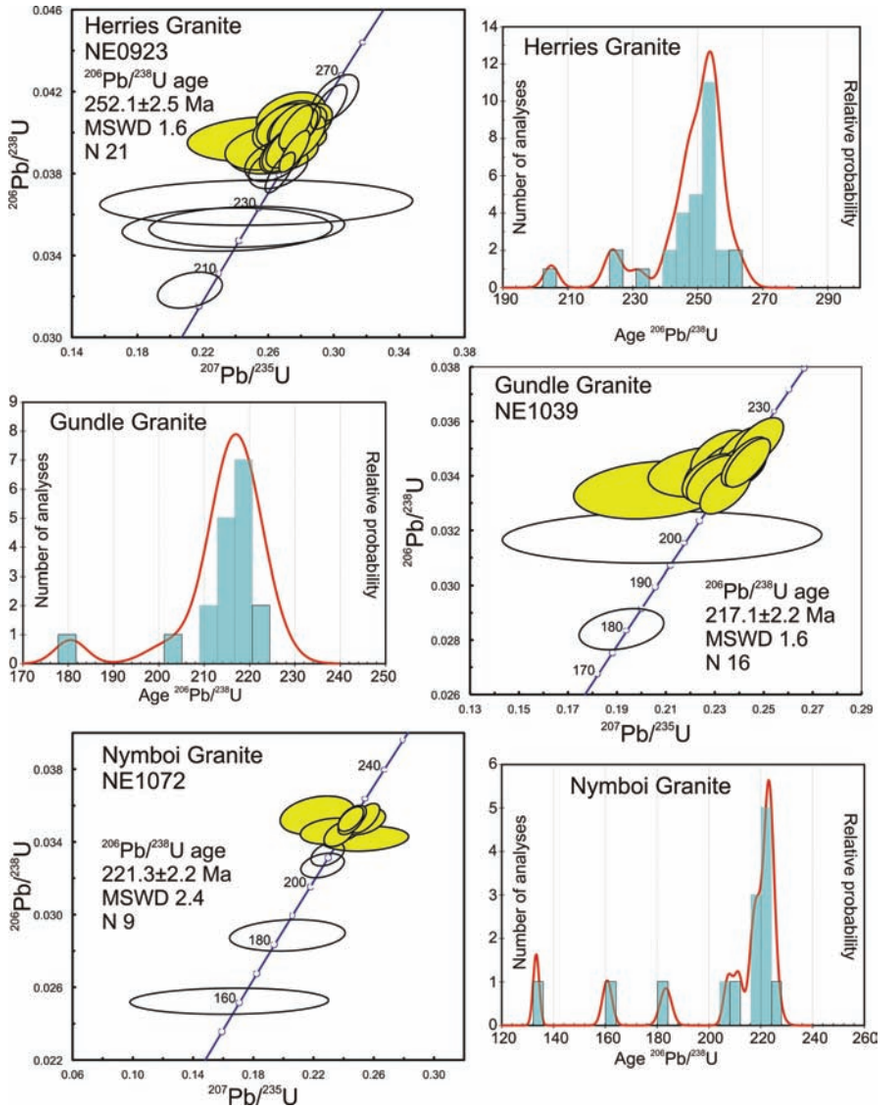

Figure 4 *Continued.*

located at the intersection between the NNE–SSW and N–S magmatic belts (Figure 1). In contrast, younger ages obtained from the Gundle Granite and Nymboi Granite, are located farther east in the southern part of N–S belt. These results, together with previously published geochronological data (Table 1), indicate that the NNE–SSW belt significantly predates the N–S belt (Figure 5). Rocks in the NNE–SSW belt are in the age range of 260–240 Ma, and do not show an internal age progression (Figure 5a, b).

We interpret the late Permian to Middle Triassic magmatic belt as the arc of a west-dipping subduction segment that, at least locally, was striking NNE–SSW (Figure 5a, b). An alternative interpretation, which is not favoured by us, is that the NNE–SSW magmatic belt is an en-echelon series of several N–S striking linear belts. This requires large displacements by strike slip faults, but the only large N–S strike-slip fault in the region is the Demon Fault that accommodated less than 30 km of dextral displacement (Figure 1). This offset is insufficient to account for the reorientation of the belt into its current NNE–SSW trend (see Figure 5a, b).

A number of observations support the idea that the late Permian to Triassic rocks in eastern Australia originated in a supra-subduction position: (1) the tonalitic I-type intrusions of the late Permian Clarence River Supersuite are characterised by cordilleran-type mineralogy, geochemistry and isotopic signature (Bryant *et al.* 1997); (2) the late Permian Emmaville Volcanics (Wandsworth Volcanic Group) have characteristic continental subduction-related geochemistry, associated with high-K calc-alkaline composition, enrichment in Al_2O_3 and LILE (Rb, K and LREE) and depletion in HFSE (Ti, Nb and Zr) (Stewart 2001); (3) late Permian shoshonites in the Sydney Basin are enriched in Al_2O_3 and LILE (Rb, K and LREE), and depleted in HFSE (Nb, Ta, Zr, Hf and Ti), Sr/Nd of ~30–35 and low Nb/U, indicating a subduction-related origin (Carr 1998); and

Table 2 SHRIMP zircon U–Pb analyses for granitoids from the southern NEO. Errors on isotopic ratios and ages are 1 sigma.

Spot Name	$^{206}Pb_c$ (%)	U (ppm)	Th (ppm)	$^{232}Th/^{238}U$	$^{207}Pb/^{235}U$	1σ %	$^{206}Pb/^{238}U$	1σ %	Error correlation	$^{206}Pb/^{238}U$ Age	1σ absolute
Fairleigh Granite											
NE0924-9.1*	0.22	990	454	0.47	0.23	2.3	0.0346	1.1	0.484	219.2	2.4
NE0924-21.1*	0.06	818	273	0.34	0.26	3.0	0.0378	1.1	0.372	239.0	2.6
NE0924-14.1*	0.18	872	307	0.36	0.26	2.1	0.0378	1.1	0.541	239.3	2.7
NE0924-1.1*	0.00	617	299	0.50	0.26	4.3	0.0387	1.1	0.261	244.8	2.7
NE0924-24.1	0.00	623	218	0.36	0.26	3.1	0.0394	1.1	0.357	249.0	2.7
NE0924-5.1	0.25	1113	492	0.46	0.28	2.4	0.0396	1.2	0.480	250.2	2.8
NE0924-3.1	0.00	1001	404	0.42	0.27	2.0	0.0396	1.1	0.532	250.6	2.7
NE0924-6.1	0.10	1166	659	0.58	0.28	1.5	0.0397	1.1	0.739	251.2	2.7
NE0924-2.1	0.02	975	435	0.46	0.28	1.6	0.0398	1.1	0.670	251.4	2.7
NE0924-7.1	0.23	899	539	0.62	0.28	2.1	0.0398	1.1	0.509	251.3	2.7
NE0924-15.1	0.09	748	277	0.38	0.28	1.8	0.0400	1.1	0.595	253.0	2.7
NE0924-4.1	0.37	785	372	0.49	0.28	3.0	0.0400	1.1	0.364	253.1	2.7
NE0924-11.1	0.01	1039	441	0.44	0.28	1.7	0.0401	1.1	0.650	253.2	2.7
NE0924-13.1	0.03	436	151	0.36	0.28	2.6	0.0401	1.1	0.430	253.3	2.8
NE0924-10.1	0.09	795	348	0.45	0.28	2.2	0.0401	1.1	0.500	253.6	2.7
NE0924-19.1	0.00	784	294	0.39	0.28	1.8	0.0402	1.2	0.640	253.8	2.9
NE0924-12.1	0.03	898	407	0.47	0.28	1.7	0.0402	1.1	0.647	253.9	2.7
NE0924-18.1	0.00	1263	575	0.47	0.27	1.8	0.0401	1.1	0.592	253.6	2.7
NE0924-23.1	0.00	929	364	0.40	0.27	2.0	0.0405	1.1	0.550	255.7	2.8
NE0924-8.1	0.04	1101	478	0.45	0.28	1.9	0.0410	1.1	0.572	259.2	2.7
NE0924-17.1	0.00	869	366	0.44	0.29	2.3	0.0414	1.1	0.468	261.5	2.8
NE0924-20.1*	0.00	442	162	0.38	0.28	4.5	0.0417	1.1	0.252	263.2	2.9
NE0924-16.1*	0.07	2463	2051	0.86	0.30	1.4	0.0420	1.1	0.774	265.0	2.8
Weighted mean										**253.3**	**2.5**
Herries Granite											
NE0923-3.1*	0.50	928	1251	1.39	0.21	3.8	0.0323	1.1	0.292	204.9	2.2
NE0923-28.1*	2.17	874	382	0.45	0.24	11.1	0.0353	1.2	0.110	223.4	2.7
NE0923-12.1*	3.11	1119	696	0.64	0.25	9.9	0.0354	1.1	0.116	224.1	2.5
NE0923-21.1*	5.58	1054	761	0.75	0.25	15.5	0.0366	1.2	0.080	231.5	2.8
NE0923-25.1*	0.05	1492	850	0.59	0.27	1.4	0.0380	1.1	0.766	240.7	2.5
NE0923-8.1*	0.41	958	1151	1.24	0.27	2.8	0.0383	1.1	0.392	242.2	2.6
NE0923-11.1*	0.38	1242	533	0.44	0.26	2.7	0.0386	1.1	0.398	244.3	2.6
NE0923-26.1	0.13	1353	658	0.50	0.28	1.4	0.0391	1.1	0.769	247.1	2.6
NE0923-30.1	0.03	708	304	0.44	0.27	2.2	0.0390	1.1	0.487	246.8	2.6
NE0923-23.1	0.91	917	530	0.60	0.26	4.2	0.0390	1.1	0.260	246.8	2.7
NE0923-13.1	0.12	1029	475	0.48	0.27	2.1	0.0392	1.2	0.555	247.8	2.8
NE0923-27.1	0.07	1022	529	0.54	0.27	2.0	0.0393	1.1	0.540	248.5	2.6
NE0923-15.1	0.17	543	212	0.40	0.26	4.0	0.0393	1.1	0.280	248.3	2.7
NE0923-7.1	0.19	1109	449	0.42	0.28	1.8	0.0397	1.1	0.609	251.2	2.8
NE0923-24.1	0.15	771	328	0.44	0.28	2.3	0.0398	1.1	0.475	251.4	2.7
NE0923-22.1	0.83	569	225	0.41	0.25	6.9	0.0397	1.1	0.165	250.8	2.8
NE0923-9.1	0.44	1424	557	0.40	0.28	2.5	0.0400	1.1	0.463	252.8	2.8
NE0923-18.1	0.01	979	342	0.36	0.28	1.7	0.0401	1.1	0.647	253.5	2.7
NE0923-29.1	0.12	727	292	0.41	0.28	2.1	0.0402	1.1	0.510	254.2	2.7
NE0923-5.1	0.14	822	346	0.44	0.27	2.8	0.0402	1.1	0.391	253.9	2.7
NE0923-19.1	0.00	653	292	0.46	0.28	1.8	0.0403	1.1	0.604	254.6	2.7
NE0923-1.1	0.03	1390	642	0.48	0.28	1.5	0.0403	1.1	0.708	254.5	2.7
NE0923-14.1	0.06	786	343	0.45	0.28	2.5	0.0403	1.1	0.445	254.5	2.7
NE0923-4.1	0.32	1017	699	0.71	0.28	2.4	0.0403	1.1	0.460	255.0	2.7
NE0923-10.1	0.00	668	287	0.44	0.27	2.1	0.0403	1.1	0.540	254.9	2.8
NE0923-16.1	0.00	704	222	0.33	0.27	2.7	0.0403	1.1	0.411	254.9	2.8
NE0923-2.1	0.16	923	589	0.66	0.27	2.7	0.0405	1.1	0.406	255.7	2.7
NE0923-6.1	0.35	918	448	0.50	0.27	3.1	0.0409	1.1	0.350	258.2	2.8
NE0923-20.1*	0.06	852	368	0.45	0.30	1.5	0.0412	1.1	0.703	260.5	2.7
NE0923-17.1*	0.10	409	102	0.26	0.30	2.0	0.0417	1.1	0.567	263.2	2.9
Weighted mean										**252.1**	**2.5**
Clare Hills Granite											
NE0927-6.1*	0.56	621	454	0.76	0.24	4.9	0.0364	1.2	0.247	230.6	2.7
NE0927-9.1*	0.35	870	482	0.57	0.25	3.3	0.0377	1.1	0.335	238.7	2.6
NE0927-24.1*	0.17	679	352	0.54	0.27	2.0	0.0381	1.1	0.548	240.8	2.6
NE0927-23.1*	0.05	931	554	0.61	0.26	2.7	0.0382	1.1	0.408	241.6	2.6

(*continued*)

Table 2 (*Continued*).

Spot Name	$^{206}Pb_c$ (%)	U (ppm)	Th (ppm)	$^{232}Th/^{238}U$	$^{207}Pb/^{235}U$	1σ %	$^{206}Pb/^{238}U$	1σ %	Error correlation	$^{206}Pb/^{238}U$ Age	1σ absolute
NE0927-11.1*	0.00	1116	504	0.47	0.26	2.0	0.0384	1.1	0.537	242.6	2.6
NE0927-26.1*	0.07	1456	669	0.47	0.27	1.5	0.0384	1.1	0.728	243.0	2.5
NE0927-21.1*	0.03	602	223	0.38	0.26	2.9	0.0387	1.1	0.378	244.8	2.7
NE0927-10.1	0.32	1677	908	0.56	0.27	2.0	0.0389	1.1	0.546	245.8	2.6
NE0927-20.1	0.00	822	353	0.44	0.26	2.5	0.0393	1.1	0.429	248.5	2.7
NE0927-25.1	0.00	636	270	0.44	0.28	1.7	0.0394	1.2	0.670	249.3	2.9
NE0927-12.1	0.12	723	427	0.61	0.27	3.0	0.0394	1.1	0.365	249.4	2.7
NE0927-3.1	0.12	1198	654	0.56	0.27	1.8	0.0395	1.1	0.583	249.9	2.6
NE0927-5.1	0.17	1160	688	0.61	0.28	2.0	0.0396	1.1	0.565	250.3	2.8
NE0927-8.1	4.64	1040	522	0.52	0.28	11.8	0.0396	1.1	0.097	250.6	2.8
NE0927-19.1	0.00	1505	607	0.42	0.27	1.7	0.0397	1.1	0.621	250.8	2.6
NE0927-4.1	0.00	931	380	0.42	0.27	2.4	0.0398	1.2	0.491	251.6	2.9
NE0927-22.1	0.00	1417	648	0.47	0.28	1.6	0.0399	1.1	0.678	252.2	2.6
NE0927-13.1	0.08	1407	632	0.46	0.28	1.5	0.0400	1.1	0.700	252.9	2.7
NE0927-17.1	0.05	2545	1209	0.49	0.28	1.4	0.0400	1.1	0.750	253.0	2.6
NE0927-18.1	0.00	1552	1160	0.77	0.28	1.8	0.0403	1.1	0.588	255.0	2.7
NE0927-7.1	0.22	1884	1231	0.68	0.28	1.9	0.0404	1.1	0.561	255.0	2.7
NE0927-1.1	0.01	691	311	0.46	0.27	3.6	0.0404	1.1	0.305	255.3	2.8
NE0927-15.1	0.06	1357	762	0.58	0.28	2.1	0.0408	1.1	0.524	257.5	2.7
NE0927-2.1	0.82	1003	395	0.41	0.28	4.1	0.0409	1.1	0.268	258.2	2.8
Weighted mean										**252.0**	**2.5**
Boonoo Granite											
NE1010-6.1*	3.55	823	563	0.71	0.24	10.0	0.0344	1.2	0.116	218.3	2.5
NE1010-10.1*	0.09	2159	289	0.14	0.26	1.4	0.0368	1.1	0.800	233.0	2.5
NE1010-8.1	0.16	1574	902	0.59	0.26	1.8	0.0377	1.2	0.650	238.4	2.7
NE1010-9.1	3.61	1025	606	0.61	0.26	20.6	0.0378	1.6	0.078	239.4	3.8
NE1010-27.1	0.36	968	759	0.81	0.27	1.9	0.0383	1.1	0.577	242.0	2.6
NE1010-3.1	0.00	204	92	0.47	0.22	5.4	0.0379	1.2	0.229	239.6	2.9
NE1010-24.1	0.05	2802	327	0.12	0.27	1.2	0.0383	1.1	0.847	242.5	2.5
NE1010-5.1	0.04	580	327	0.58	0.27	2.7	0.0385	1.1	0.417	243.4	2.7
NE1010-16.1*	9.81	809	454	0.58	0.24	35.4	0.0382	1.5	0.044	241.6	3.7
NE1010-22.1	0.25	197	128	0.67	0.28	5.3	0.0386	1.3	0.250	244.2	3.2
NE1010-26.1	0.00	468	256	0.57	0.26	2.4	0.0385	1.1	0.459	243.4	2.7
NE1010-20.1	0.01	531	302	0.59	0.27	2.4	0.0387	1.1	0.474	244.9	2.7
NE1010-13.1	0.00	529	308	0.60	0.26	2.8	0.0387	1.1	0.390	244.9	2.7
NE1010-1.1	0.22	125	60	0.50	0.22	12.9	0.0385	1.4	0.110	243.6	3.4
NE1010-21.1	0.16	317	203	0.66	0.23	6.3	0.0387	1.2	0.188	244.7	2.8
NE1010-2.1	0.00	538	634	1.22	0.27	3.2	0.0390	1.1	0.345	246.9	2.7
NE1010-25.1	0.01	880	205	0.24	0.27	1.9	0.0392	1.1	0.573	248.2	2.6
NE1010-17.1	0.09	446	201	0.46	0.28	2.2	0.0394	1.2	0.546	249.0	2.9
NE1010-28.1	0.00	537	375	0.72	0.27	2.7	0.0393	1.1	0.419	248.3	2.8
NE1010-12.1	0.19	203	206	1.05	0.26	5.8	0.0394	1.2	0.207	249.4	3.0
NE1010-14.1	0.09	734	353	0.50	0.28	2.1	0.0399	1.1	0.526	252.1	2.7
NE1010-15.1	0.13	343	242	0.73	0.27	3.3	0.0399	1.1	0.345	252.0	2.8
NE1010-11.1	0.10	932	510	0.57	0.27	2.7	0.0399	1.1	0.407	252.1	2.7
NE1010-4.1*	0.00	682	435	0.66	0.28	2.6	0.0406	1.1	0.421	256.4	2.8
NE1010-18.1*	9.89	559	343	0.63	0.22	58.7	0.0402	2.4	0.040	253.9	5.9
NE1010-7.1*	0.00	287	236	0.85	0.26	4.6	0.0413	1.5	0.324	260.9	3.8
Weighted mean										**245.6**	**2.5**
Bookookoorara Monzogranite											
NE1009-6.1*	0.64	549	282	0.53	0.23	4.8	0.0334	1.1	0.239	211.5	2.4
NE1009-1.1*	0.17	397	225	0.59	0.21	6.7	0.0361	1.2	0.177	228.8	2.6
NE1009-7.1	0.14	825	380	0.48	0.24	2.7	0.0368	1.1	0.414	232.8	2.5
NE1009-28.1	0.10	1087	546	0.52	0.26	1.8	0.0369	1.1	0.614	233.5	2.5
NE1009-16.1	0.58	1127	577	0.53	0.25	3.2	0.0370	1.1	0.356	234.5	2.6
NE1009-24.1	0.05	2288	1146	0.52	0.26	1.4	0.0375	1.1	0.752	237.2	2.5
NE1009-23.1	0.12	674	341	0.52	0.27	1.7	0.0376	1.1	0.658	237.8	2.6
NE1009-27.1	0.55	997	567	0.59	0.24	3.7	0.0374	1.1	0.291	236.6	2.5
NE1009-4.1	0.13	1312	592	0.47	0.26	1.9	0.0376	1.1	0.567	237.9	2.5
NE1009-9.1	0.15	1403	678	0.50	0.26	1.8	0.0378	1.1	0.613	239.2	2.5
NE1009-20.1	0.05	935	439	0.48	0.25	2.8	0.0378	1.2	0.415	238.9	2.8
NE1009-26.1	0.05	1065	719	0.70	0.27	1.7	0.0380	1.1	0.639	240.4	2.5
NE1009-22.1	0.11	782	351	0.46	0.26	2.4	0.0380	1.1	0.455	240.5	2.6
NE1009-8.1	0.19	1339	626	0.48	0.26	2.0	0.0381	1.1	0.534	240.8	2.5

(*continued*)

Table 2 (*Continued*).

Spot Name	$^{206}Pb_c$ (%)	U (ppm)	Th (ppm)	$^{232}Th/^{238}U$	$^{207}Pb/^{235}U$	1σ %	$^{206}Pb/^{238}U$	1σ %	Error correlation	$^{206}Pb/^{238}U$ Age	1σ absolute
NE1009-14.1	0.28	594	331	0.58	0.27	2.9	0.0383	1.1	0.386	242.1	2.7
NE1009-19.1	0.07	1318	643	0.50	0.26	1.9	0.0383	1.1	0.568	242.2	2.6
NE1009-30.1	0.02	1078	531	0.51	0.27	1.7	0.0384	1.1	0.627	243.0	2.6
NE1009-3.1	0.17	811	764	0.97	0.25	3.5	0.0383	1.1	0.314	242.4	2.6
NE1009-25.1	0.00	678	259	0.40	0.27	1.9	0.0385	1.1	0.572	243.8	2.6
NE1009-17.1	0.01	395	221	0.58	0.26	3.4	0.0385	1.1	0.334	243.6	2.7
NE1009-11.1	0.00	618	366	0.61	0.26	2.9	0.0387	1.2	0.409	245.1	2.8
NE1009-15.1	0.09	2367	697	0.30	0.27	1.4	0.0390	1.1	0.768	246.6	2.6
NE1009-13.1	0.34	2066	708	0.35	0.26	2.5	0.0389	1.1	0.435	246.0	2.6
NE1009-12.1*	0.03	539	264	0.51	0.28	1.9	0.0397	1.1	0.590	250.8	2.7
NE1009-10.1*	0.00	1498	392	0.27	0.27	1.8	0.0398	1.1	0.611	251.8	2.7
NE1009-18.1*	0.15	551	269	0.50	0.27	3.5	0.0402	1.1	0.316	254.1	2.8
NE1009-21.1*	0.09	462	244	0.55	0.28	2.7	0.0402	1.1	0.413	254.3	2.8
NE1009-29.1*	0.00	649	257	0.41	0.28	2.1	0.0404	1.1	0.522	255.2	2.7
Weighted mean										**240.1**	**2.4**
Nymboi Granite											
NE1072-6*	3.65	867	214	0.26	0.16	5.7	0.0209	0.9	0.156	133.3	1.2
NE1072-13*	2.49	1598	813	0.53	0.16	16.4	0.0252	1.2	0.071	160.7	1.8
NE1072-11*	0.91	1100	507	0.48	0.20	7.8	0.0289	1.2	0.158	183.4	2.2
NE1072-5*	0.73	1754	391	0.23	0.23	2.6	0.0327	0.8	0.326	207.5	1.7
NE1072-16*	0.00	1175	880	0.77	0.23	2.0	0.0333	0.8	0.405	211.4	1.7
NE1072-10	1.54	919	347	0.39	0.25	4.6	0.0342	0.8	0.177	216.6	1.8
NE1072-14	0.29	833	501	0.62	0.24	1.7	0.0344	0.8	0.476	218.2	1.8
NE1072-2	0.29	762	297	0.40	0.23	3.5	0.0346	0.8	0.237	219.2	1.8
NE1072-1	0.16	1534	657	0.44	0.24	1.4	0.0351	0.8	0.555	222.3	1.7
NE1072-7	0.00	469	155	0.34	0.25	2.5	0.0351	0.9	0.354	222.6	1.9
NE1072-4	0.13	956	361	0.39	0.25	1.5	0.0353	0.9	0.610	223.7	2.1
NE1072-8	0.04	1727	539	0.32	0.24	1.4	0.0353	0.8	0.554	223.4	1.7
NE1072-15	0.00	955	335	0.36	0.25	1.5	0.0353	0.8	0.526	223.7	1.8
NE1072-3	0.23	245	87	0.37	0.22	4.5	0.0355	1.2	0.269	224.7	2.7
Weighted mean										**221.3**	**2.2**
Gundle Granite											
NE1039-1*	0.67	862	337	0.40	0.19	3.7	0.0284	1.1	0.294	180.5	1.9
NE1039-11*	1.30	623	290	0.48	0.21	12.8	0.0317	1.2	0.095	201.5	2.4
NE1039-6	0.12	1020	369	0.37	0.23	1.8	0.0335	1.1	0.586	212.2	2.2
NE1039-16	0.03	407	278	0.71	0.20	6.3	0.0335	1.3	0.203	212.3	2.7
NE1039-12	0.17	1114	394	0.37	0.23	2.3	0.0339	1.1	0.470	214.6	2.2
NE1039-17	0.02	1043	440	0.44	0.23	2.0	0.0339	1.1	0.530	214.7	2.2
NE1039-5	0.03	1150	407	0.37	0.23	2.2	0.0339	1.1	0.488	215.1	2.2
NE1039-7	0.00	601	216	0.37	0.23	2.4	0.0341	1.1	0.484	216.4	2.4
NE1039-9	0.03	609	275	0.47	0.23	4.1	0.0342	1.1	0.267	216.5	2.4
NE1039-14	0.11	888	405	0.47	0.24	2.6	0.0343	1.1	0.420	217.2	2.3
NE1039-10	0.05	1260	416	0.34	0.24	1.9	0.0343	1.1	0.552	217.5	2.3
NE1039-18	0.00	811	366	0.47	0.23	2.3	0.0343	1.1	0.477	217.4	2.3
NE1039-13	0.00	875	339	0.40	0.24	2.2	0.0344	1.1	0.495	217.7	2.3
NE1039-2	0.04	910	324	0.37	0.24	1.5	0.0345	1.1	0.685	218.5	2.3
NE1039-8	0.00	953	377	0.41	0.24	1.6	0.0345	1.1	0.666	218.8	2.3
NE1039-4	0.00	1141	500	0.45	0.23	2.2	0.0348	1.1	0.481	220.4	2.3
NE1039-3	0.11	893	340	0.39	0.24	2.0	0.0349	1.1	0.536	221.3	2.3
NE1039-15	0.06	894	387	0.45	0.25	1.7	0.0352	1.1	0.617	223.1	2.3
Weighted mean										**217.1**	**2.2**

*Excluded from age calculation.

(4) late Permian ash fall in the Sydney Basin is interpreted to derive from a continental arc source on the basis of Zr/TiO_2 and Nb/Y ratios, tectonic discrimination diagrams and chondrite normalised REE patterns (La/Yb=4.05–11.37 or 3.3–11.9; Kramer *et al.* 2001; Grevenitz *et al.* 2003). The origin of the slightly older Drake Volcanics (264.4±2.5; Cross & Blevin 2010) and Barrington Tops Granodiorite (267.2±1.4 Ma; Cawood *et al.* 2011a) (Figure 5a) are more ambiguous, though they may represent the earlier history of this late Permian magmatic arc.

The exact location of this subduction zone is not clear. Cawood (1984) proposed that, prior to the opening of the Tasman Sea, the trench was located east of New

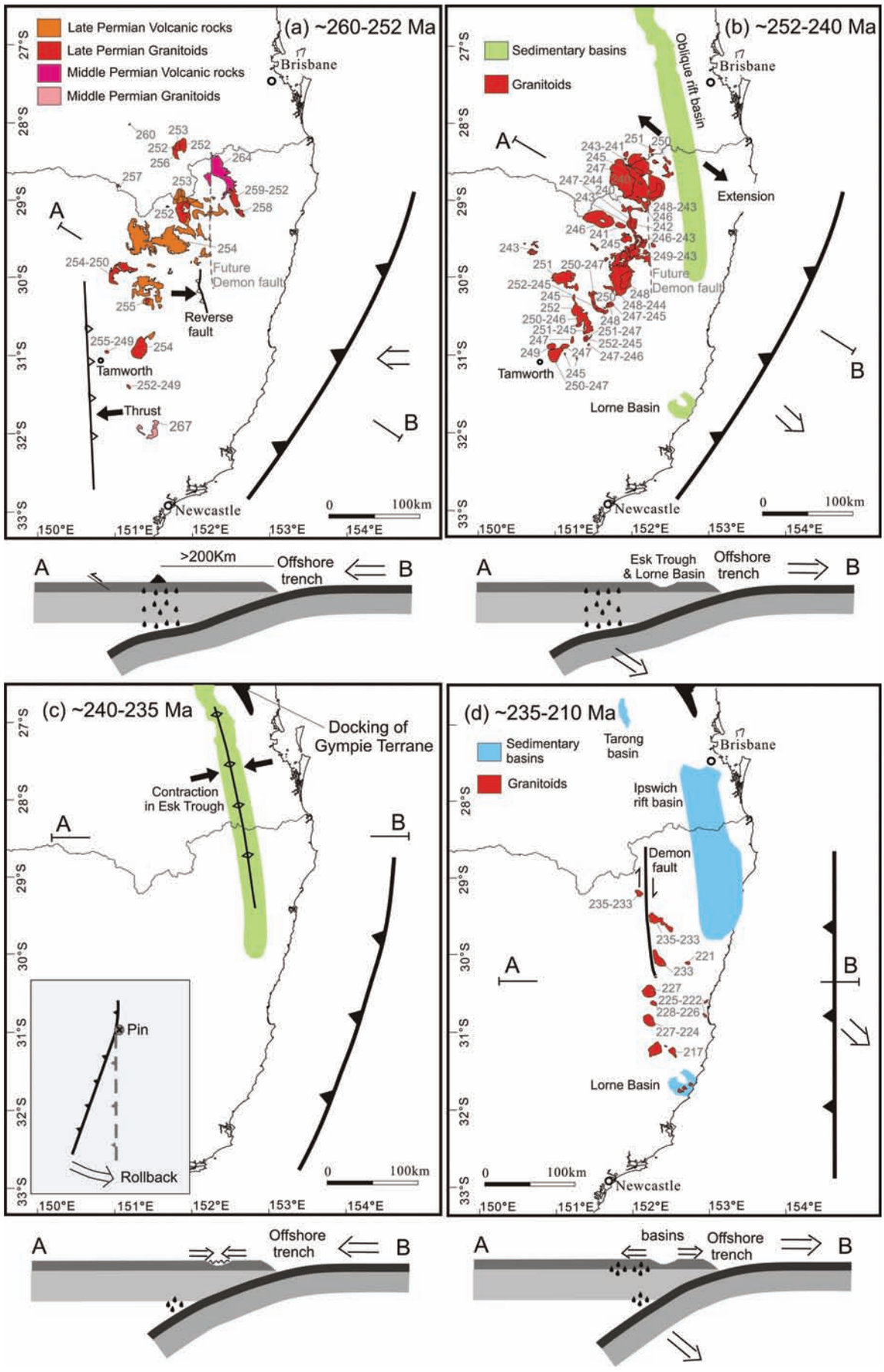

Caledonia, but this location would imply a very large trench-arc distance of ~700 km. Alternatively, it is possible that the late Permian to Triassic subduction trench was located between eastern Australia and the Lord Howe Rise (LHR). This proposal is consistent with a tectonic scenario involving the Triassic accretion of the Gympie Terrane and part of the LHR (see discussion below). The orientation of the trench is not well constrained, but was likely parallel to the NNE–SSW strike of the arc-related magmatic belt. However, the NNE–SSW magmatic belt stops around Tamworth, with no traces of Permian–Triassic magmatism farther southwest (Figures 1, 5a, b). Whether this belt and related subduction zone extended further towards SSW or bent offshore towards the coast is unclear.

The distance between the NNE–SSW igneous belt and the assumed offshore trench is >200 km, based on the distance between the magmatic belt and Australian coastline (Figure 5a). This minimum arc-trench distance is still greater than in most subduction zones (typically ~124–166 km; Stern 2002), indicating that the slab dip angle was relatively shallow. Assuming that arc magmatism was generated at the typical depth of 125 km (Stern 2002), a dip angle of <30° is required in order to account for the arc–trench distance. We therefore suggest that the late Permian subduction zone in the southern NEO was characterised by a Chilean-type shallow-dipping slab. This subduction mode, which implies strong coupling between the overriding and descending plates, may have initiated in the middle Permian (*ca* 265 Ma) and contributed to the onset of contractional deformation in the foreland areas during the early stage of the Hunter-Bowen Orogeny (Korsch *et al.* 2009c).

Triassic asymmetric rollback and the end of the Hunter-Bowen Orogeny

Late Permian to Middle Triassic magmatism in the southern NEO occurred along a NNE–SSW belt (Figures 2, 5a, b), whereas younger granitoids (*ca* 235–215 Ma) are distributed along a N–S belt farther east (Figures 2, 5d). The timing of granite emplacement along the N–S belt is coeval with the development of rift basins (e.g. the Ipswich Basin) and dextral strike-slip faulting (e.g. the Demon Fault; Figure 2). We attribute these observations to southeastward asymmetric slab rollback, whereby increasing rollback velocity in the southernmost NEO gave rise to a counter-clockwise migration in the spatial distribution of arc magmatism. Similar processes of asymmetric slab rollback, accompanied by the opening of asymmetric back-arc basins, are known in modern subduction zones, such as the New Hebrides (Auzende *et al.* 1988; Schellart *et al.* 2002), Kuril-Kamchatka (Schellart *et al.* 2003) and Tonga (Bevis *et al.* 1995). Assuming such a tectonic environment existed in the southern NEO, it is expected that asymmetric rollback was accompanied by the development of extensional basins that progressively became larger from north to south. However, with the exception of the Triassic Lorne Basin, large basins are not recognised in the southernmost NEO. Possibly, such basins exist offshore the current coast, or alternatively, it is possible that the overriding plate was not subjected to asymmetrical extension because rollback was compensated by plate convergence.

The exact timing of initiation of Triassic slab rollback in this region is not well constrained. Korsch *et al.* (1989) suggested that the Middle Triassic Esk Trough, which is located in the northern margin of the southern NEO (Figure 1), formed in response to dextral transtension. The development of this oblique rift basin, which was simultaneous with the formation of the Lorne Basin farther south, appears to be the earliest record of Triassic extension, possibly in response to the initiation of southeastward rollback (Figure 5b). This process was followed by a short period of contractional deformation and waning magmatism (*ca* 240–235 Ma, Figures 2, 5c), perhaps due to the docking of the allochthonous Gympie Terrane (Harrington & Korsch 1985; Harrington 2008). This brief contractional event was interpreted as the final stage of the Hunter-Bowen Orogeny at *ca* 241–228 Ma (Holcombe *et al.* 1997). The end of the Hunter-Bowen Orogeny could be constrained by the initial development of the N–S belt of granitoids at *ca* 235 Ma, which was accompanied by regional extension in response to southeastward slab rollback (Figures 2, 5d).

The origin of subduction rollback has been attributed to the negative buoyancy of the subducting slab relative to the surrounding asthenosphere (Elsasser 1971; Garfunkel *et al.* 1986; Kincaid & Olson 1987; Royden 1993). Pinning of the subduction zone could lead to along-strike variations in the rollback velocity and hence to asymmetric rollback. One process that could potentially pin the subduction zone is the arrival of a relatively buoyant crustal block at the subduction zone (Rosenbaum & Mo 2011). In the NEO, it is possible that such crustal anomaly is represented by the Gympie Terrane (Figure 1). The origin of the of the Gympie Terrane was proposed to be associated with the early Permian Austral Arc system (Figure 6), which may have formed by an intra-oceanic east-dipping subduction zone (Harrington & Korsch 1985; Harrington 2008).

In comparison with the rest of the NEO, the Gympie Terrane has a different tectono-stratigraphy (Day *et al.*

Figure 5 Schematic reconstruction of the late Permian to Upper Triassic subduction history in the southern NEO. Note that the spatial distribution of magmatism in (a) and (b) was restored for the ~30 km dextral offset along the Demon Fault (shown in (d)). (a) Shallow-dipping subduction during late Permian with >200 km arc–trench distance and ~E–W contractional deformation at the early stage of the Hunter-Bowen Orogeny; (b) initial stage of rollback during Lower to Middle Triassic and development of the Lorne Basin and Esk Trough; (c) Middle Triassic contraction in the Esk Trough, possibly in response to the docking of the Gympie Terrane. Inset schematic diagram shows the geometry of asymmetric rollback relative to the pinning point; and (d) continuous rollback and development of extensional basins and N–S belt of granitoids during Middle–Upper Triassic.

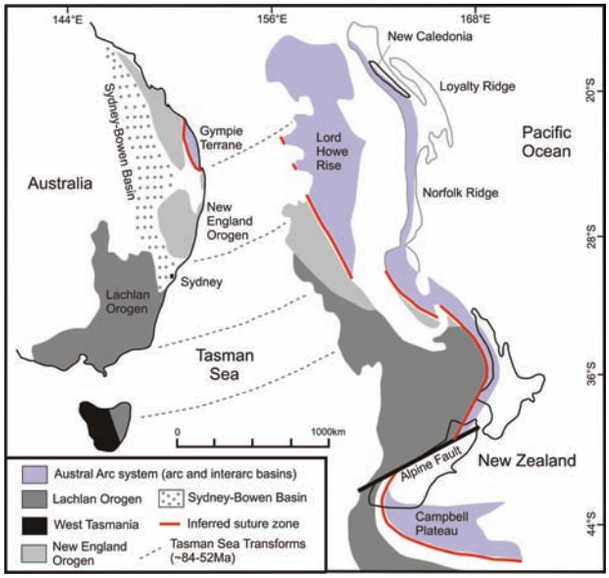

Figure 6 A schematic illustration showing possible correlations between tectonic elements in eastern Australia, Lord Howe Rise and New Zealand (after Harrington 2008). Note that according to this interpretation, the contact between the Gympie Terrane and the New England Orogen is a segment of the suture between the Australian continent and the Austral Arc system.

1978; Cranfield *et al.* 1997), and is characterised by both island-arc and mantle sourced magmatic rocks (Sivell & Waterhouse 1988; Sivell & McCulloch 1997, 2001). Detrital zircons ages from the early Permian Rammutt Formation (late Sakmarian to late Artinskian), within the Gympie Terrane, show a single peak at 276 ± 2 Ma, whereas zircons ages from the younger Keefton Formation (Induan) have multiple peaks at 252 ± 2, 318 ± 3 and 351 ± 4 Ma (Korsch *et al.* 2009a). One possible interpretation for this pattern is that accretion of the Gympie Terrane had commenced prior to the deposition of the Keefton Formation, which already received sedimentary material from the Carboniferous accretionary wedge rocks of the NEO (Korsch *et al.* 2009a). These results are consistent with the interpretation of the Gympie Terrane as an exotic block (Harrington 1974, 1983, 2008; Harrington & Korsch 1985). We argue that its accretion onto the NEO could have led to contractional deformation in the Esk Trough (Figure 5c). Moreover, the docking of this terrane may have resulted in a local decrease in the rollback velocity, giving rise to asymmetric rollback and associated counter-clockwise rotations in the southern NEO.

According to this model, part of the LHR (the Austral Arc system), together with the Gympie Terrane, were accreted to Australia in the Lower to Middle Triassic. Subsequently, in late Mesozoic and early Cenozoic, the LHR (which also included parts of the NEO and the Lachlan Orogen) was rifted away from Australia. This scenario is consistent with the correlation of terranes within the LHR, Gympie Terrane, the NEO and the Lachlan Orogen (Figure 6; Harrington 2008). We note, however, that this reconstruction implies an earlier arrival of the Gympie Terrane relative to the rest of the Austral Arc system and a cessation of subduction to the west of the LHR. Further constraints are required to support this reconstruction.

CONCLUSIONS

New U–Pb SHRIMP data from the southern NEO, complemented with previously published geochronological data, demonstrate that an older (*ca* 260–240 Ma) NNE–SSW magmatic belt predated a younger (*ca* 235–215 Ma) N–S belt farther east. Assuming that magmatism was subduction-related and was spatially distributed parallel to the subduction zone, we interpret the eastward migration in magmatism as an indicator for asymmetric slab rollback. The subduction rollback coincides with a regional tectonic switch from contraction to extension. We propose a tectonic model whereby Chilean-type shallow-dipping subduction processes, accompanied by E–W contractional deformation, accounted for the early stage of the Hunter-Bowen Orogeny. The final stage of the Hunter-Bowen Orogeny was marked by docking of the allochthonous Gympie Terrane, which pinned the subduction zone in the north and locally reduced the rate of eastward rollback, giving rise to asymmetric rollback and associated counter-clockwise rotations in the southern NEO.

ACKNOWLEDGEMENTS

Research was funded by the Australian Research Council (Grant DP0986762). The manuscript has benefited from constructive comments by the editors (Myra Keep and Wouter Schellart) and two anonymous reviewers, and discussions with Rod Holcombe and Charles Verdel.

REFERENCES

Auzende J-M., Lafoy Y. & Marsset B. 1988. Recent geodynamic evolution of the north Fiji basin (southwest Pacific). *Geology* **16**, 925–929.

Bevis M., Taylor F. W., Schutz B. E., Recy J., Isacks B. L., Helu S., Singh R., Kendrick E., Stowell J., Taylor B. & Calmantli S. 1995. Geodetic observations of very rapid convergence and back-arc extension at the Tonga arc. *Nature* **374**, 249–251.

Black L. P., Kamo S. L., Allen C. M., Aleinikoff J. N., Davis D. W., Korsch R. J. & Foudoulis C. 2003. TEMORA 1: a new zircon standard for Phanerozoic U–Pb geochronology. *Chemical Geology* **200**, 155–170.

Brownlow J. & Cross A. 2010. TIMS U–Pb and SHRIMP U–Pb zircon dating of the Dundee Rhyodacite, northern New England, NSW. *In*: Buckman S. & Blevin P. L. eds. *New England Orogen 2010.* pp. 69–74. University of New England, Armidale.

Bryant C. J., Arculus R. J. & Chappell B. W. 1997. Clarence River supersuite: 250 Ma Cordilleran tonalitic I-type intrusions in eastern Australia. *Journal of Petrology* **38**, 975–1001.

Carey S. W. & Browne W. R. 1938. Review of the carboniferous stratigraphy, tectonics and palaeogeography of New South Wales and Queensland. *Journal and Proceedings of the Royal Society of New South Wales* **71**, 591–614.

Carr P. F. 1998. Subduction-related late Permian shoshonites of the Sydney basin, Australia. *Mineralogy and Petrology* **63**, 49–71.

Cawood P. A. 1984. The development of the SW Pacific Margin of Gondwana: correlations between the Rangitata and New England Orogens. *Tectonics* **3**, 539–553.

CAWOOD P. A. 2005. Terra Australis Orogen: Rodinia breakup and development of the Pacific and Iapetus margins of Gondwana during the Neoproterozoic and Paleozoic. *Earth-Science Reviews* **69**, 249–279.

CAWOOD P. A., LEITCH E. C., MERLE R. E. & NEMCHIN A. A. 2011a. Orogenesis without collision: stabilizing the Terra Australis accretionary orogen, eastern Australia. *Geological Society of America Bulletin*. doi:10.1130/b30415.30411.

CAWOOD P. A., PISAREVSKY S. A. & LEITCH E. C. 2011b. Unraveling the New England orocline, east Gondwana accretionary margin. *Tectonics* **30**, TC5002. doi:5010.1029/2011tc002864.

COLLINS W. J. 1991. A reassessment of the 'Hunter-Bowen Orogeny': tectonic implications for the southern New England fold belt. *Australian Journal of Earth Sciences* **38**, 409–423.

COLLINS W. J. 2002. Hot orogens, tectonic switching, and creation of continental crust. *Geology* **30**, 535–538.

CRANFIELD L. C., SCHWARZBOCK H. & DAY R. W. 1976. *Geology of the Ipswich and Brisbane 1:250,000 sheet areas*. Geological Survey of Queensland Report **95**.

CRANFIELD L. C., SHORTEN G., SCOTT M. & BARKER R. M. 1997. Geology and mineralisation of the Gympie Province. *In*: Flood P. G. & Ashley P. M. eds. *Tectonics and metallogenesis of the New England Orogen*, pp. 128–147. Geological Society of Australia Special Publication **19**.

CROSS A. & BLEVIN P. 2010. Summary of results for the joint GSNSW-GA geochronology project: New England Orogen and Sydney-Gunnedah Basin April–July 2008. *Geological Survey Report* **GS2010/0778**.

DANIS C., O'NEILL C., LACKIE M., TWIGG L. & DANIS A. 2011. Deep 3D structure of the Sydney Basin using gravity modelling. *Australian Journal of Earth Sciences* **58**, 517–542.

DANIS C., O'NEILL C. & LACKIE M. A. 2010. Gunnedah Basin 3D architecture and upper crustal temperatures. *Australian Journal of Earth Sciences* **57**, 483–505.

DAY R. W., MURRAY C. G. & WHITAKER W. G. 1978. The eastern part of the Tasman Orogenic Zone. *Tectonophysics* **48**, 327–364.

DAY R. W., WHITAKER W. G., MURRAY C. G., WILSON I. H. & GRIMES K. G. 1983. *Queensland Geology. A companion volume to the 1:2,500,000 scale geological map (1975)*. Geological Survey of Queensland Publication **383**.

DE JERSEY N. J. 1972. *Triassic miospores from the Esk Beds*. Geological Survey of Queensland Publication **357**.

ELSASSER W. M. 1971. Sea-floor spreading as thermal convection. *Journal of Geophysical Research* **76**, 1101–1112.

FLINT J. C. E. & GOULD R. E. 1975. A note on the fossil megafloras of the Nymboida and Red Cliff Coal Measures, southern Clarence-Moreton Basin. *Journal and Proceedings of the Royal Society of New South Wales* **108**, 70–74.

GARFUNKEL Z., ANDERSON C. A. & SCHUBERT G. 1986. Mantle circulation and the lateral migration of subducted slabs. *Journal of Geophysical Research* **91**, 7205–7223.

GLEN R. A. 2005. The Tasmanides of eastern Australia. *In*: Vaughan A. P. M., Leat P. T. & Pankhurst R. J. eds. *Terrane processes at the margins of Gondwana*, pp. 23–96. Geological Society, London, Special Publication **246**.

GLEN R. A. & BECKETT J. 1997. Structure and tectonics along the inner edge of a foreland basin: the Hunter Coalfield in the northern Sydney Basin, New South Wales. *Australian Journal of Earth Sciences* **44**, 853–877.

GRAHAM I., SUTHERLAND L. & ZWINGMANN H. 2006. Mesozoic to Cenozoic magmatism, Lorne Basin, NSW. *18th Australian Earth Sciences Convention*. Melbourne, Australia, Extended Abstracts.

GREVENITZ P., CARR P. & HUTTON A. 2003. Origin, alteration and geochemical correlation of Late Permian airfall tuffs in coal measures, Sydney Basin, Australia. *International Journal of Coal Geology* **55**, 27–46.

GULSON B. L., DIESSEL C. F. K., MASON D. R. & KROGH T. E. 1990. High precision radiometric ages from the northern Sydney Basin and their implication for the Permian time interval and sedimentation rates. *Australian Journal of Earth Sciences* **37**, 459–469.

HARRINGTON H. J. 1974. The Tasman Geosyncline in Australia. *In*: Denmead A. K., Tweedale G. W. & Wilson A. F. eds. *The Tasman Geosyncline – a symposium*, pp. 383–407. Geological Society of Australia, Queensland Division, Brisbane.

HARRINGTON H. J. 1983. Correlation of the Permian and Triassic Gympie Terrane of Queensland with the Brook Street and Maitai terranes of New Zealand. *In*: *Permian geology of Queensland*, pp. 431–436. Geological Society of Australia, Queensland Division, Brisbane.

HARRINGTON H. J. 2008. Zealandia, Victoria, Tasmania, southeast Queensland, New Caledonia and the Austral volcanic island arc. *Transactions of the Royal Society of Victoria* **120**, v–xl.

HARRINGTON H. J. & KORSCH R. J. 1985. Late Permian to Cainozoic tectonics of the New England Orogen. *Australian Journal of Earth Sciences* **32**, 181–203.

HAYES D. E. & RINGIS J. 1973. Seafloor spreading in the Tasman Sea. *Nature* **243**, 454–458.

HELBY R. J., MORGAN R. & PARTRIDGE A. D. 1987. A palynological zonation of the Australian Mesozoic. *Association of Australian Palaeontologists, Memoir* **4**, 1–93.

HOLCOMBE R. J., STEPHENS C. J., FIELDING C. R., GUST D. A., LITTLE T. A., SLIWA R., KASSAN J., MCPHIE J. & EWART A. 1997. Tectonic evolution of the northern New England Fold Belt: the Permian–Triassic Hunter–Bowen event. *In*: Flood P. G. & Ashley P. M. eds. *Tectonics and metallogenesis of the New England Orogen*, pp. 52–65. Geological Society of Australia Special Publication **19**.

JENKINS R. B., LANDENBERGER B. & COLLINS W. J. 2002. Late Palaeozoic retreating and advancing subduction boundary in the New England Fold Belt, New South Wales. *Australian Journal of Earth Sciences* **49**, 467–489.

KINCAID C. & OLSON P. 1987. An experimental study of subduction and slab migration. *Journal of Geophysical Research* **92**, 13832–13840.

KORSCH R. 1977. A framework for the Palaeozoic geology of the southern part of the New England Geosyncline. *Australian Journal of Earth Sciences* **24**, 339–355.

KORSCH R. J., ADAMS C. J., BLACK L. P., FOSTER D. A., FRASER G. L., MURRAY C. G., FOUDOULIS C. & GRIFFIN W. L. 2009a. Geochronology and provenance of the Late Paleozoic accretionary wedge and Gympie Terrane, New England Orogen, eastern Australia. *Australian Journal of Earth Sciences* **56**, 655–685.

KORSCH R. J., ARCHER N. R. & MCCONACHY G. W. 1978. The Demon Fault. *Journal and Proceedings of the Royal Society of New South Wales* **111**, 101–106.

KORSCH R. J. & HARRINGTON H. J. 1987. Oroclinal bending, fragmentation and deformation of terranes in the New England Orogen, eastern Australia. *American Geophysical Union Geodynamics Series* **19**, 129–139.

KORSCH R. J., O'BRIEN P. E., SEXTON M. J., WAKE-DYSTER K. D. & WELLS A. T. 1989. Development of Mesozoic transtensional basins in easternmost Australia. *Australian Journal of Earth Sciences* **36**, 13–28.

KORSCH R. J., TOTTERDELL J. M., CATHRO D. L. & NICOLL M. G. 2009b. Early Permian East Australian Rift System. *Australian Journal of Earth Sciences* **56**, 381–400.

KORSCH R. J., TOTTERDELL J. M., FOMIN T. & NICOLL M. G. 2009c. Contractional structures and deformational events in the Bowen, Gunnedah and Surat Basins, eastern Australia. *Australian Journal of Earth Sciences* **56**, 477–499.

KRAMER W., WEATHERALL G. & OFFLER R. 2001. Origin and correlation of tuffs in the Permian Newcastle and Wollombi Coal Measures, NSW, Australia, using chemical fingerprinting. *International Journal of Coal Geology* **47**, 115–135.

LANDENBERGER B., FARRELL T., OFFLER R., COLLINS W. & WHITFORD D. 1995. Tectonic implications of Rb–Sr biotite ages for the Hillgrove Plutonic Suite, New England Fold Belt, NSW, Australia. *Precambrian Research* **71**, 251–263.

LEITCH E. C. 1974. The geological development of the southern part of the New England Fold Belt. *Australian Journal of Earth Sciences* **21**, 133–156.

LEITCH E. C. 1988. The Barnard Basin and the early Permian development of the southern part of the New England Fold Belt *In*: Kleeman J. D. ed. *New England Orogen – tectonics and metallogenesis*, pp. 61–67. University of New England, Armidale.

LI P., ROSENBAUM G. & DONCHAK P. J. T. 2012. Structural evolution of the Texas Orocline, eastern Australia. *Gondwana Research* **22**, 279–289.

LUDWIG K. R. 2003. *Isoplot 3.00: a geochronological toolkit for Microsoft Excel (Vol. 4)*. Berkeley Geochronology Center Special Publication, Berkeley.

McPhie J. & Fergusson C. L. 1983. Dextral movement on the Demon Fault, northeastern New South Wales: a reassessment. *Journal and Proceedings of the Royal Society of New South Wales* **116**, 123–127.

O'Brien P. E., Korsch R. J., Wells A. T., Sexton M. J. & Wake-Dyster K. 1994. Structure and tectonics of the Clarence-Moreton Basin. *In*: Wells A. T. & O'Brien P. E. eds. *Geology and petroleum potential of the Clarence-Moreton Basin, New South Wales and Queensland.* pp. 195–216. AGSO Bulletin **241**.

Offler R. & Foster D. A. 2008. Timing and development of oroclines in the southern New England Orogen, New South Wales. *Australian Journal of Earth Sciences* **55**, 331–340.

Phillips G., Landenberger B. & Belousova E. A. 2011. Building the New England Batholith, eastern Australia – linking granite petrogenesis with geodynamic setting using Hf isotopes in zircon. *Lithos* **122**, 1–12.

Pratt G. W. 2010. A revised Triassic stratigraphy for the Lorne Basin, NSW. *Quarterly Notes* **134**, 1–35.

Roach A. F. 1997. Late Triassic volcansim in the Ipswich Basin. PhD thesis, Macquarie University, Sydney.

Roberts J., Claoue-Long J. C. & Foster C. B. 1996. SHRIMP zircon dating of the Permian System of eastern Australia. *Australian Journal of Earth Sciences* **43**, 401–421.

Rosenbaum G. 2012. Oroclines of the southern New England Orogen, eastern Australia. *Episodes* **35**, 187–194.

Rosenbaum G. & Mo W. 2011. Tectonic and magmatic responses to the subduction of high bathymetric relief. *Gondwana Research* **19**, 571–582.

Rosenbaum G., Li P. & Rubatto D. 2012. The contorted New England Orogen (eastern Australia): new evidence from U–Pb geochronology of early Permian granitoids. *Tectonics* **31**, TC1006. doi:1010.1029/2011TC002960.

Royden L. H. 1993. The tectonic expression slab pull at continental convergent boundaries. *Tectonics* **12**, 303–325.

Scheibner E. 1998. *Geology of New South Wales – synthesis, volume 2, geological evolution*. Geological Survey of New South Wales Memoir Geology **13** (2).

Schellart W. P., Jessell M. W. & Lister G. S. 2003. Asymmetric deformation in the backarc region of the Kuril arc, northwest Pacific: new insights from analogue modeling. *Tectonics* **22**, 1047. doi:1010.1029/2002TC001473.

Schellart W. P., Lister G. S. & Jessell M. W. 2002. Analogue modeling of arc and backarc deformation in the New Hebrides arc and North Fiji Basin. *Geology* **30**, 311–314.

Shaw S. & Flood R. 1981. The New England Batholith, eastern Australia: geochemical variations in time and space. *Journal of Geophysical Research* **86**, 10530–10544.

Shaw S. E. & Flood R. H. 2009. Zircon Hf isotopic evidence for mixing of crustal and silicic mantle-derived magmas in a zoned granite pluton, Eastern Australia. *Journal of Petrology* **50**, 147–168.

Shaw S. E., Flood R. H. & Pearson N. J. 2011. The New England Batholith eastern Australia: evidence of silicic magma mixing from zircon $^{176}Hf/^{177}Hf$ ratios. *Lithos* **126**, 115–126.

Sivell W. J. & McCulloch M. T. 1997. Geochemistry and Sm–Nd isotope systematics of early Permian basalts from Gympie Province and fault basins in southeast Queensland: implications for mantle sources in a backarc setting at the Gondwana rim. *In*: Flood P. G. & Ashley P. M. eds. *Tectonics and metallogenesis of the New England Orogen.* pp. 148–160. Geological Society of Australia Special Publication **19**.

Sivell W. J. & McCulloch M. T. 2001. Geochemical and Nd-isotopic systematics of the Permo-Triassic Gympie Group, southeast Queensland. *Australian Journal of Earth Sciences* **48**, 377–393.

Sivell W. J. & Waterhouse J. B. 1988. Petrogenesis of Gympie Group volcanics: evidence for remnants of an early Permian volcanic arc in eastern Australia. *Lithos* **21**, 81–95.

Stacey J. S. & Kramers J. D. 1975. Approximation of terrestrial lead isotope evolution by a two-stage model. *Earth and Planetary Science Letters* **26**, 207–221.

Stern R. J. 2002. Subduction zones. *Reviews of Geophysics* **40**, 1012. doi: 1010.1029/2001RG000108.

Stewart A. L. 2001. Facies in an Upper Permian volcanic succession, Emmaville Volcanics, Deepwater, northeastern New South Wales. *Australian Journal of Earth Sciences* **48**, 929–942.

Totterdell J. M., Moloney J., Korsch R. J. & Krassay A. A. 2009. Sequence stratigraphy of the Bowen–Gunnedah and Surat basins in New South Wales. *Australian Journal of Earth Sciences* **56**, 433–459.

Waschbusch P., Korsch R. J. & Beaumont C. 2009. Geodynamic modelling of aspects of the Bowen, Gunnedah, Surat and Eromanga Basins from the perspective of convergent margin processes. *Australian Journal of Earth Sciences* **56**, 309–334.

Webb J. A. 2001. A new Marattialean fern from the Middle Triassic of Eastern Australia. *Proceedings of the Linnean Society of New South Wales* **123**, 215–224.

Williams I. S. 1998. U–Th–Pb geochronology by ion microprobe. *In*: McKibben M. A., Shanks III W. C. & Ridley W. I. eds. *Applications of microanalytical techniques to understanding mineralizing processes*, pp. 1–35. Reviews in Economic Geology Special Publication 7, Socorro.

Woodward N. B. 1995. Thrust systems in the Tamworth Zone, southern New England Orogen, New South Wales. *Australian Journal of Earth Sciences* **42**, 107–117.

Received 16 November 2011; accepted 2 April 2012